Observation of the Spin Hall Effect in Semiconductors

Y. K. Kato, *et al.*

Science **306**, 1910 (2004);
DOI: 10.1126/science.1105514

Observation of the Spin Hall Effect in Semiconductors

Y. K. Kato, R. C. Myers, A. C. Gossard, D. D. Awschalom*

Electrically induced electron-spin polarization near the edges of a semiconductor channel was detected and imaged with the use of Kerr rotation microscopy. The polarization is out-of-plane and has opposite sign for the two edges, consistent with the predictions of the spin Hall effect. Measurements of unstrained gallium arsenide and strained indium gallium arsenide samples reveal that strain modifies spin accumulation at zero magnetic field. A weak dependence on crystal orientation for the strained samples suggests that the mechanism is the extrinsic spin Hall effect.

The Hall effect (*1*, *2*) has proved to be a convenient and useful tool for probing charge transport properties in the solid state and is routinely used as a standard materials characterization method. It finds widespread application in magnetic field sensors (*2*) and has led to a wealth of new phenomena, such as the integer and fractional quantum Hall effects in two-dimensional systems (*3*, *4*), the anomalous Hall effect in ferromagnetic systems (*1*, *5*), and the spin-dependent Hall effect (*6*). In analogy to the conventional Hall effect, the spin Hall effect has been proposed to occur in paramagnetic systems as a result of spin-orbit interaction, and refers to the generation of a pure spin current transverse to an applied electric field even in the absence of applied magnetic fields. A pure spin current can be thought of as a combination of a current of spin-up electrons in one direction and a current of spin-down electrons in the opposite direction, resulting in a flow of spin angular momentum with no net charge current. Similar to the charge accumulation at the sample edges, which causes a Hall voltage in the conventional Hall effect, spin accumulation is expected at the sample edges in the spin Hall effect. Early theoretical studies predicted a spin Hall effect originating from asymmetries in scattering for up and down spins (*7*–*10*), which is referred to as an extrinsic spin Hall effect. More recently, it has been pointed out that there may exist an intrinsic spin Hall effect that arises as a result of the band structure, even in the absence of scattering (*11*, *12*). This idea has led to much theoretical discussion (*13*–*16*), but experimental evidence of the spin Hall effect has been lacking.

We report on the optical detection of the spin Hall effect in thin films of the semiconductors GaAs and InGaAs. Scanning Kerr rotation measurements show the presence of electron spin accumulation at the edges of the samples, consistent with the prediction of a spin current transverse to the applied electric field. We investigated the effect in both unstrained and strained samples and found that an applied in-plane magnetic field can play a critical role in the appearance of the spin accumulation. No marked crystal direction dependence is observed in the strained samples, which suggests that the contribution from the extrinsic spin Hall effect is dominant.

Experimental details. Experiments were performed on a series of samples fabricated from *n*-GaAs and *n*-$In_{0.07}Ga_{0.93}As$ films grown on (001) semi-insulating GaAs substrate by molecular beam epitaxy. Our results are obtained from samples fabricated from two wafers. The unstrained GaAs sample consists of 2 μm of *n*-GaAs grown on top of 2 μm of undoped $Al_{0.4}Ga_{0.6}As$, whereas the strained InGaAs sample has 500 nm of *n*-$In_{0.07}Ga_{0.93}As$ capped with 100 nm of undoped GaAs. In both wafers, the *n*-type layers are Si doped for $n = 3 \times 10^{16}$ cm^{-3} to achieve long spin lifetimes (*17*). Standard photolithography and wet etching are used to define a semiconductor channel, and the *n*-type layers are contacted with annealed Au/Ni/Au/Ge/Ni. All the samples are left attached to the 500-μm-thick substrate to minimize unintentional strain from sample mounting. Samples are placed in a low-temperature Kerr microscope (*18*) with the channel oriented perpendicular to the externally applied in-plane magnetic field B_{ext} (Fig. 1A).

Static Kerr rotation (KR) probes the electron spin polarization in the sample. A mode-locked Ti:sapphire laser produces ~150-fs pulses at a repetition rate of 76 MHz and is tuned to the absorption edge of the semiconductor. A linearly polarized beam is directed along the *z* axis and is incident normal to the sample through an objective lens with a numerical aperture of 0.73, focusing the beam to a circular spot with a full width at half-maximum of 1.1 μm. The polarization axis of the reflected beam rotates by an amount proportional to the net magnetization of the

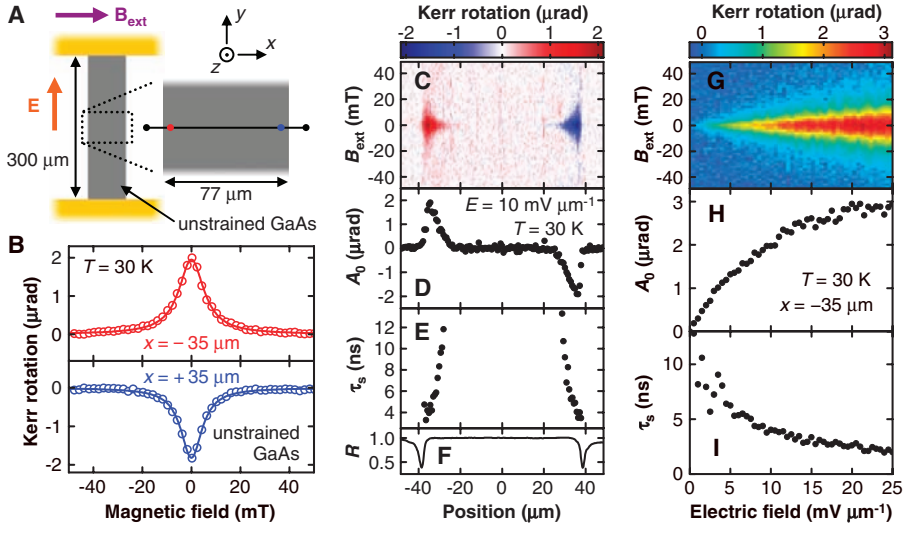

Fig. 1. The spin Hall effect in unstrained GaAs. Data are taken at $T = 30$ K; a linear background has been subtracted from each B_{ext} scan. (**A**) Schematic of the unstrained GaAs sample and the experimental geometry. (**B**) Typical measurement of KR as a function of B_{ext} for $x = -35$ μm (red circles) and $x = +35$ μm (blue circles) for $E = 10$ mV μm^{-1}. Solid lines are fits as explained in text. (**C**) KR as a function of x and B_{ext} for $E = 10$ mV μm^{-1}. (**D** and **E**) Spatial dependence of peak KR A_0 and spin lifetime τ_s across the channel, respectively, obtained from fits to data in (C). (**F**) Reflectivity R as a function of x. R is normalized to the value on the GaAs channel. The two dips indicate the position of the edges and the width of the dips gives an approximate spatial resolution. (**G**) KR as a function of E and B_{ext} at $x = -35$ μm. (**H** and **I**) E dependence of A_0 and τ_s, respectively, obtained from fits to data in (G).

Center for Spintronics and Quantum Computation, University of California, Santa Barbara, CA 93106, USA.

*To whom correspondence should be addressed. E-mail: awsch@physics.ucsb.edu

electron spins along the laser propagation direction (*19*). The KR is detected with the use of a balanced photodiode bridge with a noise equivalent power of 600 fW $Hz^{-1/2}$ in the difference channel. We apply a square wave voltage with a frequency f_E = 1.169 kHz to the two contacts, producing an alternating electric field with amplitude E for lock-in detection. Measurements are done at a temperature T = 30 K unless otherwise noted.

Detecting spin currents. An unstrained GaAs sample with a channel parallel to [110] with a width w = 77 μm, a length l = 300 μm, and a mesa height h = 2.3 μm was prepared (Fig. 1A) and was measured using a wavelength of 825 nm and an average incident laser power of 130 μW. We took the origin of our coordinate system to be the center of the channel. In Fig. 1B, typical KR data for scans of B_{ext} are shown. The red curve is taken at position x = –35 μm; the blue curve is taken at x = +35 μm, corresponding to the two edges of the channel. These curves can be understood as the projection of the spin polarization along the z axis, which diminishes with an applied transverse magnetic field because of spin precession; this is known as the Hanle effect (*8*, *20*). The data are well fit to a Lorentzian function $A_0/[(\omega_L\tau_s)^2 + 1]$, where A_0 is the peak KR, $\omega_L = g\mu_B B_{ext}/\hbar$ is the electron Larmor precession frequency, τ_s is the electron spin lifetime, g is the electron g factor (*21*), μ_B is the Bohr magneton, and $\hbar$ is the Planck constant.

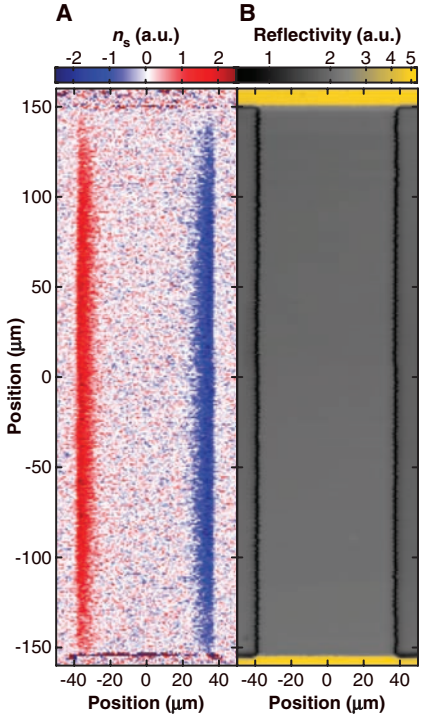

Fig. 2. (**A** and **B**) Two-dimensional images of spin density n_s and reflectivity R, respectively, for the unstrained GaAs sample measured at T = 30 K and E = 10 mV μm^{-1}.

Strikingly, the signal changes sign for the two edges of the sample, indicating an accumulation of electron spins polarized in the $+z$ direction at x = –35 μm and in the $-z$ direction at x = +35 μm. This is a strong signature of the spin Hall effect, as the spin polarization is expected to be out-of-plane and change sign for opposing edges (*7*–*12*). A one-dimensional spatial profile of the spin accumulation across the channel is mapped out by repeating B_{ext} scans at each position (Fig. 1C). It is seen that A_0, which is a measure of the spin density, is at a maximum at the two edges and falls off rapidly with distance from the edge, disappearing at the center of the channel (Fig. 1D) as expected for the spin Hall effect (*10*, *11*). We note that equilibrium spin polarization due to current-induced magnetic fields cannot explain this spatial profile; moreover, such polarization is estimated to be less than 10^{-6}, which is below our detection capability.

An interesting observation is that the width of the Lorentzian becomes narrower as the distance from the edge increases, corresponding to an apparent increase in the spin lifetime (Fig. 1E). It is possible that the finite time required for the spins to diffuse from the edge to the measurement position changes the lineshape of B_{ext} scans. Another conceivable explanation is the actual change in τ_s for spins that have diffused away from the edge. Because these spins have scattered predominantly toward the center of the channel, spin relaxation due to the D'yakonov-Perel mechanism (*20*) may be affected. In Fig. 1G, B_{ext} scans at x = –35 μm for a range of E are shown. Increasing E leads to larger spin accumulation (Fig. 1H), but the polarization saturates because of shorter τ_s for larger E (Fig. 1I). The suppression of τ_s with increasing E is consistent with previous observations (*22*).

The homogeneity of the effect is addressed by taking a two-dimensional image of the entire sample (Fig. 2, A and B). Here, instead of taking a full B_{ext} scan, B_{ext} is sinusoidally modulated at f_B = 3.3 Hz with an amplitude of 30 mT, and signal is detected at $f_E \pm 2f_B$. The measured signal is then proportional to the second derivative of a B_{ext} scan around B_{ext} = 0 mT and can be regarded as a measure of the spin density n_s. The image shows polarization localized at the two edges of the sample and having opposite sign, as discussed above. The polarization at the edges is uniform over a length of 150 μm but decreases near the contacts. The latter is expected as unpolarized electrons are injected at the contacts.

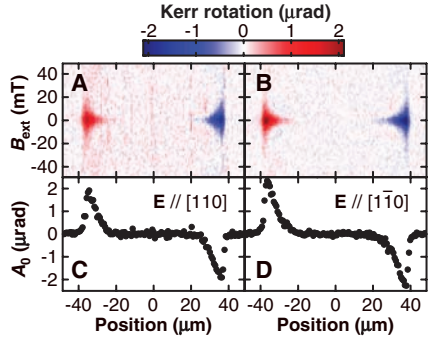

Fig. 3. Crystal orientation dependence of the spin Hall effect in the unstrained GaAs sample with w = 77 μm. (**A** and **B**) KR as a function of x and B_{ext} for E // [110] and E // [1$\bar{1}$0], respectively, with E = 10 mV μm^{-1}. A linear background has been subtracted from each B_{ext} scan. (**C** and **D**) Spatial profile of A_0 for E // [110] and E // [1$\bar{1}$0], respectively.

The origin of the observed spin Hall effect is likely to be extrinsic, as the intrinsic effect is only expected in systems with spin splitting that depends on electron wave vector k. Although k^3 spin splitting in bulk GaAs (*23*) may give rise to an intrinsic spin Hall effect, this is unlikely because negligible spin splitting has been observed in unstrained n-GaAs (*24*). Measurements were also performed on another sample with a channel parallel to [1$\bar{1}$0], and essentially the same behavior was reproduced (Fig. 3).

Effects of strain. The strained InGaAs sample, in contrast, offers the possibility of displaying the intrinsic spin Hall effect in addition to the extrinsic effect. The lattice mismatch causes strain in the InGaAs layer (*25*), and partial strain relaxation causes the in-plane strain to be anisotropic (*26*). Using reciprocal space mapping with x-ray diffraction at room temperature, we determined the in-plane strain along [110] and [1$\bar{1}$0] to be –0.24% and –0.60%, respectively, and the strain along [001] to be +0.13%. These strained layers show electron spin precession at zero applied magnetic field when optically injected electron spins are dragged with a lateral electric field (*24*), which is due to an effective internal magnetic field B_{int} perpendicular to both the growth direction and the electric field (Fig. 4A). A possible explanation for such behavior may be strain-induced k-linear spin splitting terms in the Hamiltonian, which is expected to give rise to the intrinsic spin Hall effect (*16*).

The strained InGaAs sample was processed into a channel oriented along [110] with w = 33 μm, l = 300 μm, and h = 0.9 μm. A laser wavelength of 873 nm and an incident power of 130 μW were used for this measurement, and typical results are shown in Fig. 4B. Surprisingly, the spin polarization is suppressed at B_{ext} = 0 mT, and we observe two peaks offset from B_{ext} = 0 mT. We attribute this behavior to the presence of B_{int}. Because electron spins respond to the sum of B_{ext} and B_{int}, the spin polarization is maximum at $B_{ext} = -B_{int}$ when B_{ext} cancels out B_{int}. The application of a square-wave voltage causes the signal to arise from both positive and negative electric-field directions, resulting in a double-peak structure. Although the spin polarization reverses direc-

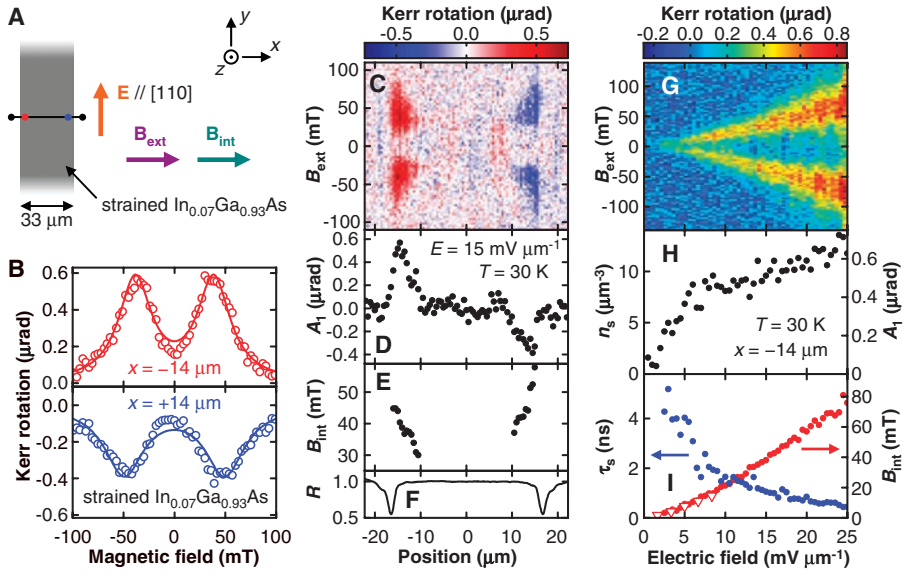

Fig. 4. The spin Hall effect in strained $In_{0.07}Ga_{0.93}As$. Data are taken at T = 30 K; a linear background has been subtracted from each B_{ext} scan. (**A**) Schematic of the strained InGaAs sample and the geometry of electric and magnetic fields. (**B**) Typical measurement of KR as a function of B_{ext} for x = −14 μm (red circles) and x = +14 μm (blue circles) for E = 15 mV μm^{-1}. Solid lines are fits as explained in text. (**C**) KR as a function of x and B_{ext} for E = 15 mV μm^{-1}. (**D** and **E**) Spatial dependence of A_1 and B_{int} across the channel, respectively, obtained from fits to data in (C). (**F**) R, normalized to the value on the InGaAs channel, as a function of x. (**G**) KR as a function of E and B_{ext} at x = −14 μm. (**H**) E dependence of n_s obtained from fits to data in (G). Corresponding A_1 are given on the right axis (*27*). (**I**) E dependence of τ_s (blue circles) and B_{int} (red circles) obtained from fits to data in (G). Red open triangles indicate B_{int} measured by spin drag experiments (*24*) on another chip from the same wafer.

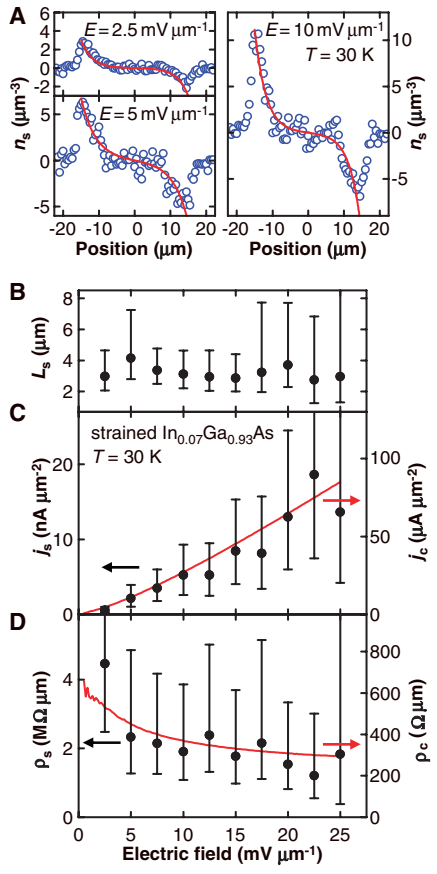

Fig. 5. (**A**) Spatial profiles of n_s for E = 2.5, 5, and 10 mV μm^{-1} at T = 30 K in the strained InGaAs sample. Blue circles are data; red lines are fits as explained in text. (**B**) L_s as a function of E obtained from fits including those shown in (A). (**C**) Spin current density j_s (black circles) and charge current density j_c (red line) as a function of E in the strained InGaAs sample. For the calculation of j_c from the total charge current measurements, an effective film thickness of 400 nm is used to take surface depletion effects into account. (**D**) Spin Hall resistivity ρ_s (black circles) and longitudinal charge resistivity ρ_c (red line) as a function of E. Changes in ρ_c with E are due to changes in the mobility originating from electronic heating, as inferred from conventional Hall measurements. The error bars in (C) and (D) include the systematic error from the calibration of n_s (*27*).

tion for opposing electric field directions, the two peaks have the same sign. This is because lock-in measurement detects the signal difference between the two electric field directions, so both positive polarization at positive E and negative polarization at negative E produce positive signal. The data are fit to $A_1/[(\omega_+\tau_s)^2 + 1] + A_1/[(\omega_-\tau_s)^2 + 1]$, where A_1 is the peak KR, and $\omega_+ = g\mu_B(B_{ext} + B_{int})/\hbar$ and $\omega_- = g\mu_B(B_{ext} - B_{int})/\hbar$ are the precession frequencies when B_{int} adds to and subtracts from B_{ext}, respectively (*21*). We note that the spatially uniform current-induced spin polarization (*22*) is not detected in this geometry, as this polarization is parallel to B_{ext}.

Spatial dependence in this sample (Fig. 4C) reproduces the characteristic signatures of the spin Hall effect. The polarization is localized at the channel edges and has opposite sign for the two edges, disappearing at the center (Fig. 4D). The slight asymmetry of the spin polarization for the two edges may be due to inhomogeneous strain. The peak width narrows as the distance from the channel edge increases, reproducing the apparent increase of τ_s in this sample as well. In addition, we find that the splitting of the two peaks decreases with increasing distance from the channel edge (Fig. 4E). A possible explanation is that the spins detected far away from the edge have average k, which has some component transverse to E; in this case, B_{int} will have a smaller component along B_{ext}, causing the splitting to decrease. The electric field dependence (Fig. 4G) exhibits similarity to the unstrained GaAs sample, showing polarization saturation (Fig. 4H) as the spin lifetime diminishes (Fig. 4I). In this sample, it is possible to correlate the KR angle to the actual spin density. We define the spin density $n_s = \langle\sigma_z\rangle n$, where $\langle\sigma_z\rangle$ is the expectation value of the Pauli operator and n is the electron density. To obtain a calibration for n_s, we used the Kerr microscope to measure the current-induced spin polarization in a sample from the same wafer with known characteristics (*27*). The peak spin density reaches 10 μm^{-3}, a value comparable to that of current-induced spin polarization. The electric field dependence of B_{int} is also plotted in Fig. 4I, and it shows very similar values to the B_{int} measured by spin drag experiments (*24*) on another chip from the same wafer. Additional measurements between 10 K < T < 60 K with E = 15 mV μm^{-1} show no marked changes in the spin polarization or its spatial profile.

It is possible to calculate the spin current from the values of the accumulated spin density. In a simple picture ignoring the position dependence of τ_s, the solution to the spin drift-diffusion equation (*10*, *11*) is $n_0 \sinh(x/L_s)/\cosh[w/(2L_s)]$, where $n_0 = \iota_s\tau_s/L_s$ is the spin density at the edge, $L_s = (D_s\tau_s)^{1/2}$ is the spin diffusion length, D_s is the spin diffusion coefficient, $\iota_s = \langle\sigma_z v\rangle n$ is the spin current density, and v is the velocity operator. By fitting the spatial dependence for various values of E (Fig. 5A), we obtain both n_0 and L_s. Values of τ_s are averaged between 10 μm < x < 15 μm for the calculations of ι_s. We note that L_s does not change noticeably with E (Fig. 5B), whereas τ_s decreases with increasing E. This implies that D_s increases with E, consistent with previous measurements (*24*). In Fig. 5C, we plot the spin current density $j_s = e\iota_s$, where e is the unit charge. The spin current is converted into units of charge current to allow comparison with the longitudinal charge current density j_c, which is also plotted in Fig. 5C. The spin Hall resistivity $\rho_s = E/j_s$ and the longitudinal charge resistivity $\rho_c = E/j_c$ are plotted in Fig. 5D. The intrinsic spin Hall resistivity,

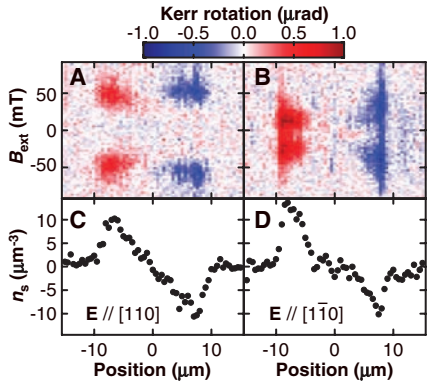

Fig. 6. Crystal orientation dependence of the spin Hall effect in the strained InGaAs sample with w = 18 μm. (**A** and **B**) KR as a function of x and B_{ext} for E // [110] and E // [1$\bar{1}$0], respectively, with E = 15 mV μm^{-1}. A linear background has been subtracted from each B_{ext} scan. (**C** and **D**) Spatial profile of n_s obtained from the fits for E // [110] and E // [1$\bar{1}$0], respectively.

when neglecting the effect of scattering, is predicted to be $4\pi^2\hbar/(e^2k_F) = 1.69$ kilohm·μm, where k_F is the Fermi wave vector (*16*); the measured values are ~2 megohm·μm. We estimate the effect of scattering by noting that a factor of $(\Delta\tau/\hbar)^2$ enters the expression for spin current (*14*), where Δ is the spin splitting at the Fermi energy and τ is the momentum relaxation time. Although this result is derived for other systems, this factor is ~10^{-6} for our samples and may explain why the observed spin current is small.

In an effort to identify a possible contribution from the intrinsic effect, we investigated crystal orientation dependence. The spin splitting in these strained InGaAs samples has crystal anisotropy (*24*), and therefore the intrinsic contribution should be sensitive to the crystal axis. Samples oriented along [110] and [1$\bar{1}$0] were fabricated on a single chip to minimize the effect of inhomogeneous strain. The results are shown in Fig. 6, where we observe that the splitting of the two peaks is smaller for E // [1$\bar{1}$0] because B_{int} is smaller in this direction (*24*), whereas no marked difference in n_s is seen, which suggests that the extrinsic effect is also dominant in the strained InGaAs samples.

Conclusion. The observed spin Hall effect provides new opportunities for manipulating electron spins in nonmagnetic semiconductors without the application of magnetic fields. The spin current and spin accumulation induced by the spin Hall effect may be used to route spin-polarized current depending on its spin, or to amplify spin polarization by splitting a channel into two and cascading such structures. In addition, the suppression of spin accumulation at B_{ext} = 0 mT caused by B_{int} is an important aspect that has not been considered previously and may possibly allow control of the spin accumulation by means of, for example, gate voltage control of the Rashba effect (*28*).

References and Notes

1. C. L. Chien, C. R. Westgate, Eds., *The Hall Effect and Its Applications* (Plenum, New York, 1980).
2. R. S. Popovic, *Hall Effect Devices* (Institute of Physics, Bristol, UK, ed. 2, 2004).
3. B. Huckestein, *Rev. Mod. Phys.* **67**, 357 (1995).
4. H. L. Stormer, D. C. Tsui, A. C. Gossard, *Rev. Mod. Phys.* **71**, S298 (1999).
5. W. L. Lee, S. Watauchi, V. L. Miller, R. J. Cava, N. P. Ong, *Science* **303**, 1647 (2004).
6. J. N. Chazalviel, *Phys. Rev. B* **11**, 3918 (1975).
7. M. I. D'yakonov, V. I. Perel, *JETP Lett.* **13**, 467 (1971).
8. M. I. D'yakonov, V. I. Perel, *Phys. Lett. A* **35**, 459 (1971).
9. J. E. Hirsch, *Phys. Rev. Lett.* **83**, 1834 (1999).
10. S. Zhang, *Phys. Rev. Lett.* **85**, 393 (2000).
11. S. Murakami, N. Nagaosa, S. C. Zhang, *Science* **301**, 1348 (2003).
12. J. Sinova *et al.*, *Phys. Rev. Lett.* **92**, 126603 (2004).
13. E. I. Rashba, *Phys. Rev. B* **68**, 241315(R) (2003).
14. J. Schliemann, D. Loss, *Phys. Rev. B* **69**, 165315 (2004).
15. J. Inoue, G. E. W. Bauer, L. W. Molenkamp, *Phys. Rev. B* **70**, 041303(R) (2004).
16. B. A. Bernevig, S. C. Zhang, www.arXiv.org/abs/cond-mat/0408442 (2004).
17. J. M. Kikkawa, D. D. Awschalom, *Phys. Rev. Lett.* **80**, 4313 (1998).
18. J. Stephens *et al.*, *Phys. Rev. B* **68**, 041307(R) (2003).
19. S. A. Crooker, D. D. Awschalom, J. J. Baumberg, F. Flack, N. Samarth, *Phys. Rev. B* **56**, 7574 (1997).
20. F. Meier, B. P. Zakharchenya, Eds., *Optical Orientation* (Elsevier, Amsterdam, 1984).
21. The electron g factor is –0.44 for the unstrained GaAs sample and –0.63 for the strained InGaAs sample, as determined by time-resolved Faraday rotation measurements (*19*).
22. Y. K. Kato, R. C. Myers, A. C. Gossard, D. D. Awschalom, *Phys. Rev. Lett.* **93**, 176601 (2004).
23. G. Dresselhaus, *Phys. Rev.* **100**, 580 (1955).
24. Y. Kato, R. C. Myers, A. C. Gossard, D. D. Awschalom, *Nature* **427**, 50 (2004).
25. S. C. Jain, M. Willander, H. Maes, *Semicond. Sci. Technol.* **11**, 641 (1996).
26. K. L. Kavanagh *et al.*, *J. Appl. Phys.* **64**, 4843 (1988).
27. The strained InGaAs sample is the sample E used in previous work (*22*, *24*). We use the value of current-induced spin polarization efficiency η as defined in (*22*) to obtain the calibration, and assume that the ratio of KR to spin polarization is within 10% on the samples from the same wafer that are measured in these experiments. The systematic error introduced in this calibration is +48%/–38%.
28. J. Nitta, T. Akazaki, H. Takayanagi, T. Enoki, *Phys. Rev. Lett.* **78**, 1335 (1997).

29. Supported by the Defense Advanced Research Projects Agency, the Defense Microelectronics Activity, and NSF.

21 September 2004; accepted 28 October 2004
Published online 11 November 2004;
10.1126/science.1105514
Include this information when citing this paper.

REPORTS

Transient Interface Sharpening in Miscible Alloys

Zoltán Erdélyi,[1]* Marcel Sladecek,[3] Lorenz-M. Stadler,[3] Ivo Zizak,[4] Gábor A. Langer,[1] Miklós Kis-Varga,[2] Desző L. Beke,[1] Bogdan Sepiol[3]

We observed that diffuse interfaces sharpen rather than broaden in completely miscible ideal binary systems. This is shown in situ during heat treatments at gradually increasing temperatures by scattering of synchrotron radiation in coherent Mo/V multilayers containing initially diffuse interfaces. This effect provides a useful tool for the improvement of interfaces and offers a way to fabricate better x-ray or neutron mirrors, microelectronic devices, or multilayers with giant magnetic resistance.

Computer simulations have recently shown (*1*, *2*) that on the nanoscale, for strongly composition-dependent diffusion coefficients, an initially diffuse interface of species A and B can become chemically abrupt even in ideal (either crystalline or amorphous) systems with complete mutual solubility. This sharpening is surprising at first sight, because the direction of diffusion is always opposite to the direction of the composition gradient: $J = -D$ grad c, where J is the atomic flux, D is the diffusion coefficient, and c is the concentration. Indeed, for constant D, the composition profile will gradually decay and a broadening of the interface is expected. However, when the diffusion coefficient is strongly dependent on the local composition, the flux distribution can lead to a sharpening of the interface (Fig. 1). For example, the sharpening can occur when the diffusion of A and B in B is much faster than the diffusion of either in A. The sharpening can be qualitatively predicted from the classical Fick I law, although it is not able to provide correct kinetics on the nanoscale (*1*, *3*).